

Superconducting-Gravimeter Tests of Local Lorentz Invariance

Natasha A. Flowers, Casey Goodge, and Jay D. Tasson

Physics and Astronomy Department, Carleton College, Northfield, Minnesota 55057, USA

(Received 9 February 2017; revised manuscript received 28 July 2017; published 16 November 2017)

Superconducting-gravimeter measurements are used to test the local Lorentz invariance of the gravitational interaction and of matter-gravity couplings. The best laboratory sensitivities to date are achieved via a maximum-reach analysis for 13 Lorentz-violating operators, with some improvements exceeding an order of magnitude.

DOI: 10.1103/PhysRevLett.119.201101

Local Lorentz invariance is among the foundational building blocks of general relativity (GR). Though GR provides an impressive description of the wide variety of gravitational phenomena, standard lore holds that GR may be the low-energy limit of an underlying theory that merges gravitation and quantum physics, such as string theory. Local Lorentz violation may arise in such an underlying framework [1]. Hence, tests of local Lorentz invariance probe the core construction of GR and may provide clues about the structure of new physics at the quantum-gravity scale. These ideas triggered the development of a comprehensive effective field theory based framework [2,3] for testing Lorentz symmetry used in many modern searches for violations [4].

Superconducting gravimeters [5] have generated a vast amount of information about the gravitational field of Earth. Devices functioning at over two dozen locations around the globe generate data at minute intervals for the Global Geodynamics Project [6]. In some cases measurements span more than a decade, and sensitivities to local variations in the gravitational field approaching parts in 10^{12} can be extracted for variations with periods on the order of a day. Stability at the level of parts in 10^9 per year [5] has also been achieved. Though the primary use of the data is in geophysical applications, the nature of the data clearly also depends on the foundational theories of physics. Hence, these data sets provide opportunities to test fundamental physics [7,8]. The search for preferred frame effects in gravitational physics, a particular Lorentz-symmetry violating scenario, was perhaps the first application of superconducting gravimeters to tests of foundational theory [9].

In the four decades since those early tests, interest in Lorentz violation has surged [10], as have theoretical and experimental developments [11–13]. In addition to the search for preferred frame effects as a signal of alternatives to GR [14], more general types of Lorentz violation are now actively sought as a possible signal of new physics at the Planck scale [4]. Though performing Planck-scale experiments directly will likely remain infeasible for the foreseeable future, experimental information about the nature of the underlying theory can be attained by searching for tiny Planck-suppressed effects in experiments at presently accessible energies. Lorentz violation provides a useful candidate

Planck-suppressed effect [1], and the gravitational standard-model extension (SME) provides a field-theory based framework for organizing a systematic search [2,3,15]. While sensitivities to SME coefficients for Lorentz violation have been achieved in a variety of gravitational systems [16–23], including pioneering work with an atom-interferometer gravimeter [16,17], this work provides the first exploration of superconducting gravimeters in the SME framework and the first search for matter-sector Lorentz violation using gravimeters of any kind. Sensitivity improvements over prior gravimeter work [16,17] are achieved for seven coefficients for Lorentz violation, and the best laboratory sensitivity to six coefficients not previously explored in gravimeter experiments is achieved. In some cases, sensitivities are improved by more than a factor of 10.

The SME is constructed as an expansion about the actions of GR and the standard model in Lorentz-violating operators of increasing mass dimension. In the present work we focus on the minimal gravitational SME, in which attention is restricted to operators of mass dimension 3 and 4. We consider both the pure-gravity sector [24] and the spin-independent gravitationally coupled fermion sector [25] in the limit of linearized gravity. Though work extending the framework to include higher dimension operators [22,23,26] and nonlinear gravity [27] is now well underway, treatment of these operators lies beyond our present scope. Here, we summarize aspects of the SME framework relevant for this work. For additional detail, the reader is referred to Refs. [3,24,25].

The SME action in this limit can be written $S = S_G + S_\psi + S'$. Here, S_G is the minimal pure-gravity sector,

$$S_G = \frac{1}{16\pi G} \int d^4x e (R - uR + s^{\mu\nu} R_{\mu\nu} + t^{\kappa\lambda\mu\nu} C_{\kappa\lambda\mu\nu}), \quad (1)$$

where G is Newton's constant, and R , $R_{\mu\nu}$, and $C_{\kappa\lambda\mu\nu}$ are the Ricci scalar, Ricci tensor, and Weyl tensor, respectively. The symbol e is the determinant of the vierbein e_μ^a , and u , $s^{\mu\nu}$, and $t^{\kappa\lambda\mu\nu}$ are coefficient fields having dynamics contained in S' . Lorentz violating signals in the post-Newtonian analysis to follow are associated with $s^{\mu\nu}$, without contribution from $t^{\kappa\lambda\mu\nu}$ [28].

Similarly, spin-independent effects in the minimal gravitationally coupled fermion sector take the form

$$S_\psi = \int d^4x \left(\frac{1}{2} i e e^\mu_{a} \bar{\psi} \Gamma^a \overleftrightarrow{D}_\mu \psi - e \bar{\psi} M \psi \right). \quad (2)$$

Here, ψ is the fermion field and D_μ is the covariant derivative, which, along with the vierbein, provides the coupling to gravity, $\Gamma^a \equiv \gamma^a - c_{\mu\nu} e^{\nu a} e^\mu_b \gamma^b - e_\mu e^{\mu a}$, and $M \equiv m + a_\mu e^\mu_a \gamma^a$. The matter-sector coefficient fields a_μ , e_μ , and $c_{\mu\nu}$ also have dynamics contained within S' . The dynamics are assumed to trigger spontaneous Lorentz violation in which the coefficient fields acquire vacuum expectation values, a process for generating Lorentz violation in gravity that is consistent with Riemann geometry [3,29]. The issue of geometric consistency has also led to the development of SME-based Finsler spacetimes [30].

The vacuum expectation values, or coefficients for Lorentz violation, are denoted with an overline and, though other choices are possible [31], are typically assumed constant in asymptotically Minkowski spacetimes. For example, the vacuum value associated with the coefficient field $c_{\mu\nu}$ is $\bar{c}_{\mu\nu}$ satisfying $\partial_\alpha \bar{c}_{\mu\nu} = 0$. The coefficients parametrize the amount of Lorentz violation in the theory and are the objects sought by experiment. Following generic treatment of spontaneous Lorentz violation and the development of the post-Newtonian limit in the pure-gravity sector [24] and the matter sector [25], the signals for Lorentz violation in gravitational experiments can be found. In the work to follow, the coefficients for Lorentz violation \bar{a}_μ and \bar{e}_μ always appear in the combination $(\bar{a}_{\text{eff}})_\mu = \bar{a}_\mu - m \bar{e}_\mu$. Additionally, $(\bar{a}_{\text{eff}})_\mu$ appears with a constant α in gravitational studies, which characterizes coupling constants in the underlying theory. This combination is of special interest since it is typically unobservable in flat spacetime [32]. Note also that the matter-sector coefficients are in general particle-species dependent and a superscript w denotes the associated species. In this work, the focus is on ordinary matter with w referring to a proton, neutron, or electron.

The system of interest here can be referred to as a force-comparison gravimeter experiment [25]. In this class of experiments, the gravitational force on a laboratory body is countered by an appropriate electromagnetic force, and the Lorentz-violating signal can be written

$$F_{LV} = -m^\top g \sum_n [A_n \cos(\omega_n T + \phi_n) + B_n \sin(\omega_n T + \phi_n)], \quad (3)$$

as developed in Sec. VIIC of Ref. [25], where

$$\begin{aligned} A_n &= \sum_w \left(\frac{N^w}{m^\top} G_n^w + \frac{N_\oplus^w}{m^S} E_n'^w + \frac{1}{3} G_n \right), \\ B_n &= \sum_w \left(\frac{N^w}{m^\top} H_n^w + \frac{N_\oplus^w}{m^S} F_n'^w + \frac{1}{3} H_n \right). \end{aligned} \quad (4)$$

Here, g is the Newtonian gravitational field, m^\top and m^S are the conventional Lorentz-invariant mass of the test body and source body, respectively, and N^w and N_\oplus^w are the number of particles of type w in the test body and Earth, respectively. Here, the test body is a niobium sphere with a mass of a few grams, and the source body is Earth. The summation index w takes the values proton, neutron, and electron. The frequencies ω_n are drawn from the set

$$\omega_n \in \{2\omega, \omega, 2\omega + \Omega, 2\omega - \Omega, \omega + \Omega, \omega - \Omega, \Omega\}, \quad (5)$$

where ω is the sidereal angular frequency and Ω is the annual angular frequency. Note that 2ω arises due to the rotation of two-index coefficients. The corresponding phase ϕ_n can be obtained from the frequency via the replacement $\omega \rightarrow \phi$, $\Omega \rightarrow 0$, where ϕ is a phase that specifies the orientation of the laboratory at time $T = 0$. The time T along with the spacial coordinates X, Y, Z are the coordinates of the Sun-centered celestial equatorial frame in standard use for SME studies [4]. The contributions to the Lorentz-violating amplitude $G_n^w, H_n^w, E_n'^w$, and $F_n'^w$ can be found in Table I, while the contributions G_n and H_n are constructed via Eq. (142) of Ref. [25]. These are the results developed in Ref. [25] presented here with a few corrections. Here, $V_L = \omega R$, where R is Earth's radius and V_\oplus is the speed of Earth on its path around the Sun. The angle ζ is between the local Lorentz-invariant free-fall direction and the direction of Earth's center, χ is the colatitude of the experiment, η is the inclination of Earth's orbit, and m^w is the mass of species w .

Our method for extracting measurements of the coefficients for Lorentz violation from the Global Geodynamics Project data proceeds as follows. We use corrected minute data, which provide a measurement of the gravitational force each minute obtained from the raw data via some repairs performed by the station manager including the removal of some transients such as major earthquakes. Where possible, we follow the methods developed for the atom-interferometer gravimeter analysis [16]. The basic idea is to perform a discrete Fourier transform on relevant sets of gravitational force versus time data to extract the amplitudes A_n, B_n . Equation (4) is then used to interpret the amplitudes as measurements of the SME coefficients.

As is typical of SME searches, the amplitudes A_n, B_n extracted from data collected by a particular device at a given site provide a measurement of a linear combination of SME coefficients rather than a measurement of a single term in the underlying theory. The numbers multiplying the coefficients for Lorentz violation in these linear combinations can contain the colatitude of the experiment χ and the dependence on the particle species content of the bodies involved. Hence, different sets of data from different locations and/or different devices measure different linear combinations of SME coefficients. Two procedures are common in the literature for extracting sensitivities to

TABLE I. Amplitudes for the force F_{LV} .

Amplitude	Phase
$G_{\omega}^w = 2m^w \zeta(\bar{c}^w)_{(XZ)} - \frac{4}{5} V_L \alpha(\bar{a}_{\text{eff}}^w)_Y \sin \chi - 2m^w V_L (\bar{c}^w)_{(TY)} \sin \chi$	ϕ
$+ \frac{4}{5} V_L \alpha(\bar{a}_{\text{eff}}^w)_X \sin \chi + 2m^w V_L (\bar{c}^w)_{(TX)} \sin \chi$	ϕ
$G_{2\omega}^w = m^w \zeta((\bar{c}^w)_{XX} - (\bar{c}^w)_{YY})$	2ϕ
$H_{2\omega}^w = 2m^w \zeta(\bar{c}^w)_{(XY)}$	2ϕ
$G_{\Omega}^w = 2V_{\oplus} \alpha((\bar{a}_{\text{eff}}^w)_Y \cos \eta + (\bar{a}_{\text{eff}}^w)_Z \sin \eta) + 2m^w V_{\oplus} [(\bar{c}^w)_{(TY)} \cos \eta + 2(\bar{c}^w)_{(TZ)} \sin \eta]$	0
$H_{\Omega}^w = -2V_{\oplus} \alpha(\bar{a}_{\text{eff}}^w)_X - 2m^w V_{\oplus} (\bar{c}^w)_{(TX)}$	0
$E_{\omega}^w = -V_L (2\alpha(\bar{a}_{\text{eff}}^w)_Y + \frac{4}{5} m^w (\bar{c}^w)_{(TY)}) \sin \chi$	ϕ
$F_{\omega}^w = V_L (2\alpha(\bar{a}_{\text{eff}}^w)_X + \frac{4}{5} m^w (\bar{c}^w)_{(TX)}) \sin \chi$	ϕ
$E_{\Omega}^w = 2V_{\oplus} \alpha((\bar{a}_{\text{eff}}^w)_Y \cos \eta + (\bar{a}_{\text{eff}}^w)_Z \sin \eta) + 2m^w V_{\oplus} [(\bar{c}^w)_{(TY)} \cos \eta + (\bar{c}^w)_{(TZ)} \sin \eta]$	0
$F_{\Omega}^w = -2V_{\oplus} \alpha(\bar{a}_{\text{eff}}^w)_X - 2m^w V_{\oplus} (\bar{c}^w)_{(TX)}$	0

individual SME coefficients from such linear combinations. One approach effectively considers a series of special models, each involving one and only one nonzero coefficient for Lorentz violation, hence attributing the measurement of an amplitude A_n , B_n to each of the coefficients it contains individually. This approach is motivated by the thinking that exact cancellation between multiple coefficients in a given measurement is unlikely. We call sensitivities to coefficients for Lorentz violation obtained in this way the “maximum reach” achieved for the given coefficient. The other approach is to treat all coefficients as nonzero simultaneously and use multiple sets of data to separate the linear combinations. We say sensitivities attained in this way are found by “coefficient separation.” In what follows we apply both methods using several sets of gravimeter data.

For our maximum-reach analysis we used data from Bad Homburg, Germany, from 2007–2013 (with several gaps of less than one week), a site providing some of the cleanest data. Three days of original gravimeter data from Bad Homburg are shown in Fig. 1, appearing as the large-amplitude signal.

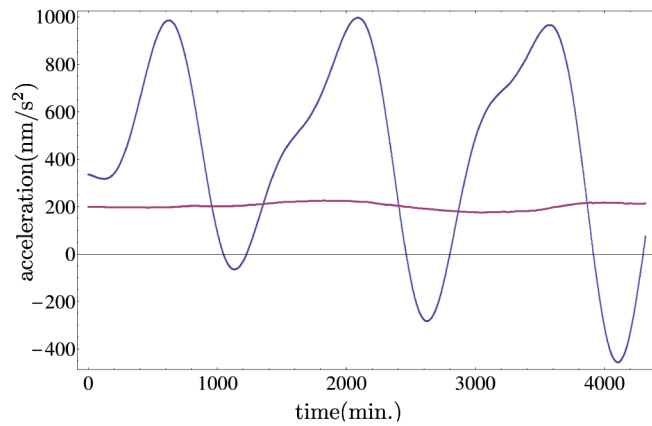


FIG. 1. Bad Homburg data taken January 1–3, 2012, before and after tidal model subtraction. Discrete points are plotted that appear as a continuous curve at this scale.

A daily variation associated with tidal effects is clearly visible in the three peaks. Following Ref. [16] we remove the dominate tidal contributions from the signal using a model of solid Earth tides [33]. Figure 1 also shows the data after the subtraction of the model. Application of a discrete Fourier transform to the residuals,

$$A_n, B_n = \frac{2}{K} \sum_k d(t_k) \cos, \sin(\omega_n t_k + \phi), \quad (6)$$

yields the amplitudes shown in Table II. Here, K is the total number of measurements; $d(t_k)$ are the residual gravity measurements at times t_k . Estimated uncertainties are obtained following Refs. [16,17] by performing the analysis at several frequencies near the characteristic frequencies and computing the root mean square.

The amplitudes in Table II together with the maximum-reach procedure yield the sensitivities to the coefficients for Lorentz violation shown in the second column of Table III. A dagger (\dagger) indicates a sensitivity that exceeds previous laboratory tests, though better constraints exist from Solar System or astrophysical observations [19–21,23,34]. The maximum reach listed here for the $\bar{s}^{\mu\nu}$ coefficients, which have previously been explored via gravimeter analysis [16,17], is an improvement upon that work for all seven coefficients listed.

TABLE II. Bad Homburg amplitudes.

Amplitude	Measurement ($10^{-9}g$)	Amplitude	Measurement ($10^{-9}g$)
$A_{2\omega}$	-0.02 ± 0.01	$B_{2\omega}$	0.04 ± 0.01
A_{ω}	-0.01 ± 0.06	B_{ω}	-0.1 ± 0.1
$A_{2\omega+\Omega}$	-0.003 ± 0.004	$B_{2\omega+\Omega}$	0.003 ± 0.004
$A_{2\omega-\Omega}$	-0.01 ± 0.01	$B_{2\omega-\Omega}$	0.006 ± 0.005
$A_{\omega+\Omega}$	-0.00 ± 0.02	$B_{\omega+\Omega}$	-0.01 ± 0.02
$A_{\omega-\Omega}$	0.01 ± 0.03	$B_{\omega-\Omega}$	0.06 ± 0.03
A_{Ω}	-1 ± 1	B_{Ω}	1 ± 1

TABLE III. Lorentz violation measurements.

Coefficient	Max reach via Bad Homburg	Four-site coefficient separation
\bar{s}^{XX-YY}	$2 \pm 1 \times 10^{-10}^\dagger$	\dots
\bar{s}^{XY}	$-4 \pm 1 \times 10^{-10}^\dagger$	\dots
\bar{s}^{XZ}	$0 \pm 1 \times 10^{-10}^\dagger$	$-2 \pm 2 \times 10^{-9}^\dagger$
\bar{s}^{YZ}	$3 \pm 1 \times 10^{-10}^\dagger$	$4 \pm 3 \times 10^{-9}^\dagger$
\bar{s}^{TX}	$-3 \pm 3 \times 10^{-7}^\dagger$	$-3 \pm 3 \times 10^{-7}^\dagger$
\bar{s}^{TY}	$-6 \pm 3 \times 10^{-7}^\dagger$	$-5 \pm 2 \times 10^{-7}^\dagger$
\bar{s}^{TZ}	$-1 \pm 1 \times 10^{-6}^\dagger$	$-1 \pm 1 \times 10^{-6}^\dagger$
$(\bar{c}^n)_{(TX)}$	$-4 \pm 6 \times 10^{-6}$	$-3 \pm 2 \times 10^{-3}$
$(\bar{c}^n)_{(TY)}$	$-1 \pm 1 \times 10^{-5}$	$2 \pm 4 \times 10^{-3}$
$(\bar{c}^n)_{(TZ)}$	$-1 \pm 1 \times 10^{-5}$	\dots
$\alpha(\bar{a}_{\text{eff}}^{e+p})_X$	$-4 \pm 6 \times 10^{-6} \text{ GeV}^\dagger$	$3 \pm 2 \times 10^{-2} \text{ GeV}$
$\alpha(\bar{a}_{\text{eff}}^n)_X$	$-4 \pm 5 \times 10^{-6} \text{ GeV}^\dagger$	$-3 \pm 2 \times 10^{-2} \text{ GeV}$
$\alpha(\bar{a}_{\text{eff}}^{e+p})_Y$	$-5 \pm 7 \times 10^{-6} \text{ GeV}^\dagger$	$0 \pm 4 \times 10^{-2} \text{ GeV}$
$\alpha(\bar{a}_{\text{eff}}^n)_Y$	$-4 \pm 6 \times 10^{-6} \text{ GeV}^\dagger$	$0 \pm 3 \times 10^{-2} \text{ GeV}$
$\alpha(\bar{a}_{\text{eff}}^{e+p})_Z$	$-1 \pm 2 \times 10^{-5} \text{ GeV}^\dagger$	\dots
$\alpha(\bar{a}_{\text{eff}}^n)_Z$	$-1 \pm 1 \times 10^{-5} \text{ GeV}^\dagger$	\dots

We perform the same analysis on data collected from the device in Metsahovi, Finland, from 2007–2012, and on a year’s worth of data from Strasbourg, France and from Apache Point, USA taken in 2012. While the maximum reach available from these sites is typically less than that obtained from Bad Homburg, their locations at different colatitudes permit some coefficient separation. We do this following the procedure outlined in Ref. [17] in which each measurement of A_n , B_n provides a probability distribution that we assume to be Gaussian with the measurement and uncertainty providing the center and standard deviation. The probability distribution can then be understood as a function of the coefficients for Lorentz violation through Eq. (4). These probability distributions can then be multiplied together for each of the relevant measurements from each of the four sites to obtain an overall probability distribution. Integrating the distribution over all of the coefficients except the one of interest then yields an estimate and uncertainty for that coefficient. The result of this process provides our estimates for the coefficients achieved by coefficient separation shown in the right column of Table III. This procedure for achieving initial coefficient separation estimates assumes the error sources in the four experiments are completely independent, while some geophysical noise sources may be somewhat coherent. Though beyond our current scope, it may be possible to address this potential issue through coherent combination of the original data. Relative to Ref. [17], correlations between amplitudes due to finite data are small and are neglected here.

Coefficients \bar{s}^{XX-YY} and \bar{s}^{XY} are obtained from amplitudes in which they are the only coefficient for the Lorentz violation involved. Hence, these entries in the maximum reach column of Table III could equally be regarded as the results of coefficient separation, and they are omitted from the

four-site analysis. Sufficient information is not available to separate the $\alpha(\bar{a}_{\text{eff}}^{e+p})_Z$, $\alpha(\bar{a}_{\text{eff}}^n)_Z$, and $(\bar{c}^n)_{TZ}$ coefficients from each other. Hence, individual constraints are not available for column 3 of Table III, and the combination is treated as a single coefficient in the separation analysis resulting in $\alpha(\bar{a}_{\text{eff}}^{e+p})_Z + 1.1\alpha(\bar{a}_{\text{eff}}^n)_Z + 1.1 \text{ GeV}(\bar{c}^n)_{TZ} = 0 \pm 6 \times 10^{-4} \text{ GeV}$. We do not include data from other experiments beyond the four gravimeter sites except in excluding from consideration other coefficients that have been constrained much more tightly by nongravitational tests. As this work was completed, the $(\bar{c}^n)_{TJ}$ were also constrained by nongravitational tests [35]. Note that the results of coefficient separation generate improvements over prior lab work for $\bar{s}^{\mu\nu}$ coefficients while constraints for matter-sector coefficients are weak. This feature can be traced to the fact that all four sites involve niobium test masses and Earth and hence the same proton/neutron ratios. Note also that proton and electron coefficients are listed together as separating them would require charged data.

The sensitivities to coefficients in Table III, found via the standard approach to gravimeter analysis in the SME [16,17], provide a basic sense of upper bounds on coefficients. However, some care should be used in interpreting the results. Though we find no compelling evidence of Lorentz violation, some notable deviations from zero are seen in a few cases. In addition to the statistical expectation of a few weak signals when seeking this number of effects, these likely reflect some challenges inherent to the search that we outline here.

The search involves subtracting dominant tidal effects from the gravimeter signal and attributing any remaining periodicity at the characteristic frequencies to Lorentz violation, with uncertainty estimated by the average level of the local Fourier spectrum near the characteristic frequency. The method relies on the assumption that any potential Lorentz-violating signal is not also contained in the tidal model. Modeling of additional local effects is avoided to minimize this concern. We also note that a Fourier transform of the raw data with no tidal modeling yields the same level of reach for annual variations, which is the aspect of the measurement associated with many of the most significant sensitivity improvements. The method also assumes that residual environmental effects at the characteristic frequencies have a size similar to neighboring Fourier amplitudes. This assumption is most challenged by Lorentz-violating frequencies that coincide with dominant tidal components. Here, the relatively small residual signal is the result of subtracting a comparatively large modeled tide from a similarly sized signal. One could also imagine the Lorentz-violation signal of a special linear combination of coefficients that matches the tidal phase being masked by a tidal effect.

A variety of opportunities for further improvements with related experiments exist. One key challenge in gravimeter tests is managing periodic environmental effects without

using models constructed by fitting to gravimeter data. A way to side step this issue for matter-sector coefficients is to consider analogous weak-equivalence principle tests that search for a variation in the relative gravitational force or acceleration of two or more bodies. It may also be possible to use the phase information associated with environmental systematics to separate them from the effects of certain combinations of coefficients for Lorentz violation. Correlations between signals at multiple sites may also be useful. Gravimeter data involving bodies of other compositions would aid in performing coefficient separation for the matter sector. Free-fall gravimeter tests such as atom interferometers are also of interest, particularly for the matter sector, as they involve a different dependence on the matter-sector coefficients. An increase in the long-term stability of gravimeters would further improve sensitivities at the annual frequency. Beyond gravimeters, searches for Lorentz violation with satellite geodesy data may be of interest. In all, exciting prospects remain for further searches for Lorentz violation with gravimeters and related systems.

This work was supported in part by the Carleton College Clinton Ford Physics Research Fund.

-
- [1] V. A. Kostelecký and S. Samuel, *Phys. Rev. D* **39**, 683 (1989).
- [2] D. Colladay and V. A. Kostelecký, *Phys. Rev. D* **55**, 6760 (1997); **58**, 116002 (1998).
- [3] V. A. Kostelecký, *Phys. Rev. D* **69**, 105009 (2004).
- [4] V. A. Kostelecký and N. Russell, arXiv:0801.0287v9.
- [5] J. M. Goodkind, *Rev. Sci. Instrum.* **70**, 4131 (1999).
- [6] The Global Geodynamics Project, <http://www.eas.slu.edu/GGP/ggphome.html>; J. Hinderer and D. Crossley, *J. Geodyn.* **48**, 299 (2009).
- [7] S. Shiomu, *Prog. Theor. Phys. Suppl.* **172**, 61 (2008).
- [8] M. Coughlin and J. Harms, *Phys. Rev. D* **90**, 042005 (2014).
- [9] K. Nordtvedt and C. M. Will, *Astrophys. J.* **177**, 775 (1972); R. J. Warburton and J. M. Goodkind, *Astrophys. J.* **208**, 881 (1976).
- [10] *Proceedings of the Seventh Meeting on CPT and Lorentz Symmetry*, edited by V. A. Kostelecký (World Scientific, Singapore, 2017).
- [11] For reviews of the SME approach, see, and J. D. Tasson, *Rep. Prog. Phys.* **77**, 062901 (2014); R. Bluhm, *Lect. Notes Phys.* **702**, 191 (2006).
- [12] For a review of the SME gravity sector, see, A. Hees, Q. G. Bailey, A. Bourgoin, H. Pihan-Le Bars, C. Guerlin, and C. Le Poncin-Lafitte, *Universe* **2**, 30 (2016).
- [13] For discussion of other approaches to Lorentz violation see, for example, S. Liberati, *Classical Quantum Gravity* **30**, 133001 (2013); S. Mirshekari, N. Yunes, and C. M. Will, *Phys. Rev. D* **85**, 024041 (2012).
- [14] For a review, see C. M. Will, *Theory and Experiment in Gravitational Physics* (Cambridge University Press, Cambridge, England, 1993).
- [15] V. A. Kostelecký and M. Mewes, *Phys. Rev. D* **80**, 015020 (2009); **85**, 096005 (2012); **88**, 096006 (2013).
- [16] H. Müller, S. W. Chiow, S. Herrmann, S. Chu, and K.-Y. Chung, *Phys. Rev. Lett.* **100**, 031101 (2008).
- [17] K. Y. Chung, S. W. Chiow, S. Herrmann, S. Chu, and H. Müller, *Phys. Rev. D* **80**, 016002 (2009).
- [18] D. Bennett, V. Skavysh, and J. Long, in *CPT and Lorentz Symmetry V*, edited by V. A. Kostelecký (World Scientific, Singapore, 2010); J. B. R. Battat, J. F. Chandler, and C. W. Stubbs, *Phys. Rev. Lett.* **99**, 241103 (2007); Q. G. Bailey, R. D. Everett, and J. M. Overduin, *Phys. Rev. D* **88**, 102001 (2013); H. Panjwani, L. Carbone, and C. C. Speake, in *CPT and Lorentz Symmetry V*, edited by V. A. Kostelecký (World Scientific, Singapore, 2010); J. D. Tasson, *Phys. Rev. D* **86**, 124021 (2012); M. A. Hohensee, H. Müller, and R. B. Wiringa, *Phys. Rev. Lett.* **111**, 151102 (2013); H. Müller, S. W. Chiow, S. Herrmann, S. Chu, and K. Y. Chung, *Phys. Rev. Lett.* **100**, 031101 (2008); M. A. Hohensee, S. Chu, A. Peters, and H. Müller, *Phys. Rev. Lett.* **106**, 151102 (2011); C.-G. Shao, Y.-J. Tan, W.-H. Tan, S.-Q. Yang, J. Luo, and M. E. Tobar, *Phys. Rev. D* **91**, 102007 (2015); J. C. Long and V. A. Kostelecký, *Phys. Rev. D* **91**, 092003 (2015); N. Yunes, K. Yagi, and F. Pretorius, *Phys. Rev. D* **94**, 084002 (2016); M. Schreck, *Classical Quantum Gravity* **34**, 135009 (2017); C. Le Poncin-Lafitte, A. Hees, and S. Lambert, *Phys. Rev. D* **94**, 125030 (2016); A. Bourgoin *et al.*, arXiv:1607.00294; C.-G. Shao *et al.*, *Phys. Rev. Lett.* **117**, 071102 (2016); A. Hees *et al.*, *Universe* **2**, 30 (2016); J. D. Tasson, *Symmetry* **8**, 111 (2016).
- [19] A. Bourgoin, A. Hees, S. Bouquillon, C. Le Poncin-Lafitte, G. Francou, and M.-C. Angonin, *Phys. Rev. Lett.* **117**, 241301 (2016).
- [20] A. Hees, Q. G. Bailey, C. Le Poncin-Lafitte, A. Bourgoin, A. Rivoldini, B. Lamine, F. Meynadier, C. Guerlin, and P. Wolf, *Phys. Rev. D* **92**, 064049 (2015).
- [21] L. Shao, *Phys. Rev. Lett.* **112**, 111103 (2014); *Phys. Rev. D* **90**, 122009 (2014).
- [22] V. A. Kostelecký and M. Mewes, *Phys. Lett. B* **757**, 510 (2016).
- [23] V. A. Kostelecký and J. D. Tasson, *Phys. Lett. B* **749**, 551 (2015).
- [24] Q. G. Bailey and V. A. Kostelecký, *Phys. Rev. D* **74**, 045001 (2006).
- [25] V. A. Kostelecký and J. D. Tasson, *Phys. Rev. D* **83**, 016013 (2011).
- [26] V. A. Kostelecký and M. Mewes, *Phys. Lett. B* **766**, 137 (2017); Q. G. Bailey, V. A. Kostelecký, and R. Xu, *Phys. Rev. D* **91**, 022006 (2015).
- [27] Q. G. Bailey, *Phys. Rev. D* **94**, 065029 (2016); M. D. Seifert, arXiv:1608.01642.
- [28] Y. Bonder, *Phys. Rev. D* **91**, 125002 (2015).
- [29] R. Bluhm, *Phys. Rev. D* **91**, 065034 (2015); **92**, 085015 (2015); R. Bluhm and A. Sehic, *Phys. Rev. D* **94**, 104034 (2016).
- [30] V. A. Kostelecký, *Phys. Lett. B* **701**, 137 (2011); V. A. Kostelecký, N. Russell, and R. Tso, *Phys. Lett. B* **716**, 470 (2012); J. E. G. Silva, arXiv:1602.07345; M. Schreck, *Phys. Rev. D* **94**, 025019 (2016); J. Foster and R. Lehnert, *Phys. Lett. B* **746**, 164 (2015); A. B. Aazami and M. A. Javaloyes, *Classical Quantum Gravity* **33**, 025003 (2016); X. Li and S. Wang, *Eur. Phys. J. C* **76**, 51 (2016); E. Caponio and G. Stanciarone, *Int. J. Geom. Methods Mod. Phys.* **13**, 1650040 (2016).

- (2016); E. Minguzzi, *Rep. Math. Phys.* **77**, 45 (2016); N. Russell, *Phys. Rev. D* **91**, 045008 (2015); D. Colladay and P. McDonald, *Phys. Rev. D* **92**, 085031 (2015).
- [31] C. D. Lane, *Phys. Rev. D* **94**, 025016 (2016).
- [32] V. A. Kostelecký and J. D. Tasson, *Phys. Rev. Lett.* **102**, 010402 (2009).
- [33] H.-G. Wenzel, ETGTAB3.0 solid earth tide data generation software, <http://www.bfo.geophys.uni-stuttgart.de/etgtab.html>.
- [34] B. Altschul, *Phys. Rev. D* **78**, 085018 (2008).
- [35] H. Pihan-LeBars, C. Guerlin, R. D. Lasserri, J. P. Ebran, Q. G. Bailey, S. Bize, E. Khan, and P. Wolf, *Phys. Rev. D* **95**, 075026 (2017).